PHILOSOPHICAL MAGAZINE A, 1999, VOL. 79, NO. 7, 1655–1669

Mechanism and crystallography of ferrite precipitation from cementite in an Fe–Cr–C alloy during austenitization

D. V. SHTANSKY†, K. NAKAI and Y. OHMORI

Department of Materials Science and Engineering, Ehime University, 3 Bunkyo-cho, Matsuyama 790-8577, Japan

[*Received 13 July 1998 and accepted in revised form 11 September 1998*]

ABSTRACT

The morphology of ferrite precipitates formed within cementite and the mechanism of their formation were examined by means of transmission electron microscopy in an Fe–2.6 wt% Cr–0.96 wt% C alloy after austenitizing in the range 800–950°C for various times. At the beginning of the austenitization process, the cementite particles dissolve rapidly by carbon diffusion in the austenite. The precipitation of ferrite occurs during the second stage of transformation when cementite dissolution is controlled by chromium diffusion in cementite or in the austenite matrix. The ferrite precipitates exhibit a lath-like shape elongated in the [010] cementite direction with the habit plane close to the (001) cementite. The cementite and ferrite were related to each other by two previously reported orientation relationships. In the case of the Pitsch–Petch orientation relationship, the habit plane of the ferrite lath is almost parallel to $(152)_f // (001)_c$ and the ferrite–cementite interface is flat without any steps. The side facet of the lath is close to $(215)_f // (101)_c$, and the ferrite growth direction is close to $[311]_f // [010]_c$. In the case of the Bagaryatsky orientation relationship, the habit plane of the ferrite lath deviates several degrees from the broad face of $(112)_f // (001)_c$ and structural ledges form at the ferrite–cementite interface, preserving coherency. The side facet of the lath is close to $(121)_f // (101)_c$ and the ferrite growth direction is close to $[111]_f // [010]_c$. The results are discussed by assuming local equilibrium at the moving interfaces using the software THERMOCALC.

§1. INTRODUCTION

The dissolution of cementite may take various forms depending on the temperature and the chemical composition. It has also been shown that a second phase often precipitates within cementite via an *in-situ* mechanism. According to Okamoto and Matsumoto (1975), when an unalloyed or a dilute-alloyed white cast iron is held at subcritical temperatures in the range 500–800°C, fine ferrite particles precipitate as platelets within the eutectic cementite. Inoue and Masumoto (1980) presented direct experimental evidence of the *in-situ* transformation from cementite to M_7C_3 in high-carbon chromium steel during tempering at 600°C. Liu *et al.* (1991) reported the transformation of cementite particles into austenite, in Fe–Cr–C alloys during austenitization, by a Widmanstätten type of reaction, or into M_7C_3 and austenite by a

† On leave from the I. P. Bardin Iron and Steel Industry Institute, Second Baumanskaya Street, 9/23, Moscow 107005, Russia.

Philosophical Magazine A ISSN 0141–8610 print/ISSN 1460-6992 online
http://www.tandf.co.uk/JNLS/phm.htm
http://www.taylorandfrancis.com/JNLS/phm.htm

eutectoid reaction. In their experiments, austenite transformed into martensite during quenching. Lyasotsky and Shtansky (1993) observed either retained austenite or martensite plates within cementite after laser heat treatment in an Fe–1.5 wt% Cr–C alloy and a white cast iron. They divided the observed reaction into three stages: the formation of stacking faults on (001) cementite planes, the precipitation of austenite preferentially on lattice defects and finally the formation of a ledeburite-type structure. Precipitation of a new phase of bct structure within cementite has also been reported by Lyasotsky and Shtansky (1993) but the composition of this phase has not been determined.

It should also be noted that the theories describing the ferrite (Okamoto and Matsumoto 1975) and austenite (Liu *et al.* 1991, Lyasotsky and Shtansky 1993) precipitation are somewhat different. According to Okamoto and Matsumoto (1975), the ferrite particles develop by excluding carbon atoms from the cementite lattice at high temperatures. Lyasotsky and Shtansky (1993) developed the same idea for the explanation of austenite precipitation in cementite whereas Liu *et al.* (1991) assumed chromium supersaturation in cementite and did not consider the carbon diffusion in cementite. In most cases, it is rather difficult to conclude what phase forms at the austenitizing temperature because the austenite formed within cementite may transform to martensite during subsequent quenching. However, examination of the defect structure at the cementite–ferrite interface will clarify whether the ferrite was formed by a diffusional mechanism or is martensitic ferrite produced by decomposition of austenite.

The present study was, therefore, undertaken in order to clarify what happens to cementite during austenitization. Particular attention is given to the mechanism and the crystallography of the formation of a second phase inside the cementite.

§2. Experimental details

The chemical composition of the alloy used in the present investigation is shown in table 1. This composition allows us to obtain the cementite–ferrite duplex structure with the maximum solubility of chromium in cementite by long time annealing. Specimens of 20 mm diameter and 10 mm long were austenitized at 1150°C for 15 min in a dynamic argon atmosphere and then quenched into iced brine. These specimens were sealed in evacuated quartz tubes, isothermally held at 735°C for 240 h and finally quenched into iced brine. This treatment resulted in the initial microstructure consisting of spherical or globular cementite particles of about 1–2 μm in a ferrite matrix.

Specimens of dimensions 10 mm × 10 mm × 0.3 mm were sliced from the centre of each heat-treated cylinder, again austenitized at different temperatures in the range 800–950°C for various times between 1 and 100 s and then quenched into iced brine. For austenitizing times as long as 1000 and 10 000 s, bulk specimens of dimensions 80 mm × 80 mm × 80 mm were used. The specimens for the microstructural investigations were sliced from the centre of each bulk specimen. Austenitization was performed in a salt bath. Thin foils for transmission electron

Table 1. Chemical composition of the alloy.

Element	C	Si	Mn	P	S	Cr	N	O	Al
Amount (wt%)	0.95	0.03	0.02	0.001	0.001	2.61	0.0015	0.001	0.002

microscopy (TEM) studies were prepared from 3 mm discs, ground to a thickness of about 0.05 mm and electropolished by a conventional twin-jet polishing method using an electrolyte containing 10% perchloric acid, 20% glycerol and 70% ethanol. The foils were examined in a JEM-3010 transmission electron microscope operating at 300 kV.

§3. Experimental results

Austenitizing experiments were carried out at three different temperatures, namely 800, 900 and 950°C. The compositions of the alloy fall into three-phase γ + cementite + M_7C_3, two-phase γ + M_7C_3 or one-phase γ areas at these temperatures respectively. The microstructures of the cementite after heat treatment at 900°C for 100 s and 950°C for 10–30 s are very similar and will be considered below.

Figure 1 shows fine precipitates within cementite after holding at 900°C for 100 s. These precipitates were identified as ferrite by selected area diffraction (SAD) and

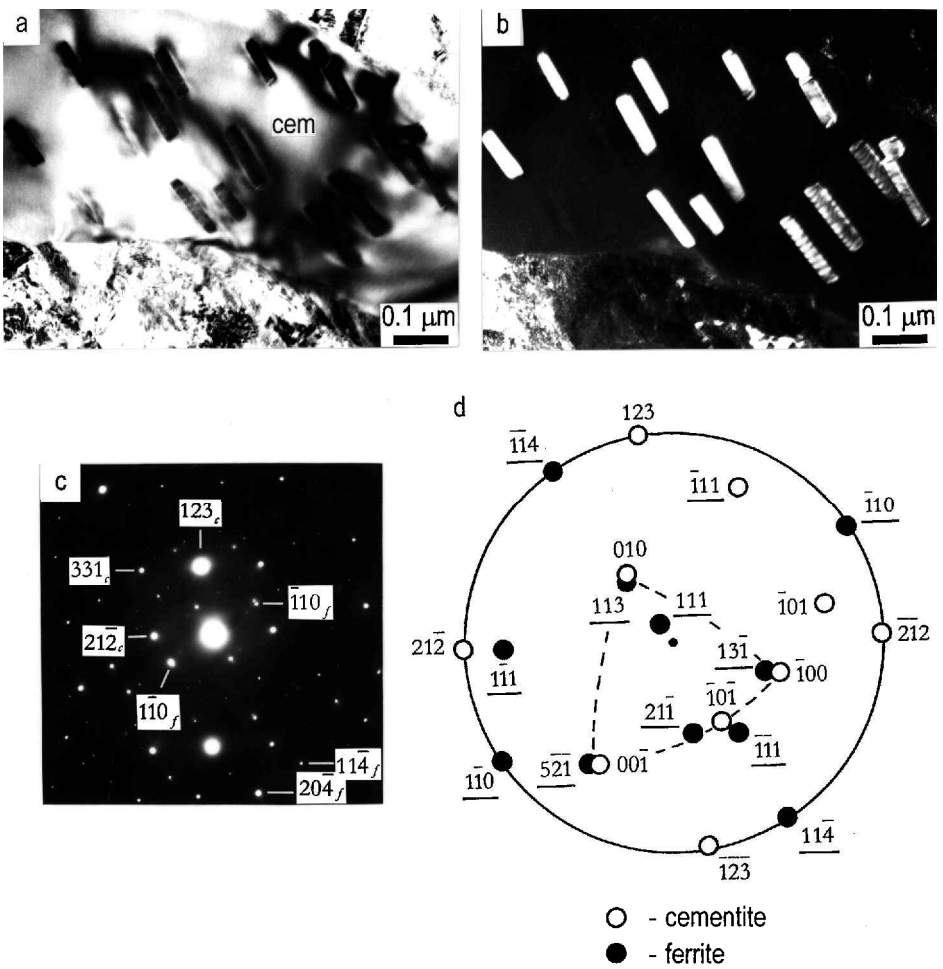

Figure 1. (*a*) BF image and (*b*) DF image using the $\bar{1}10_f$ reflection showing the ferrite precipitates within the cementite after heat treatment at 900°C for 100 s. (*c*) SAD pattern and (*d*) its stereographic analysis. Additional reflections are due to the double diffraction. This is the Pitsch–Petch orientation relationship.

the dark field DF image using a $\bar{1}10$ ferrite reflection. The particle distribution in cementite is rather inhomogeneous. From the crystallographic analysis, the following orientation relationship between ferrite and cementite was deduced:

$$(00\bar{1})_c // (5\bar{2}\bar{1})_f, (010)_c \approx // (113)_f, (\bar{1}00)_c \approx // (13\bar{1})_f,$$

which is the Pitsch–Petch (1953) orientation relationship (hereafter, the subscripts c and f denote cementite and ferrite respectively).

The bright field (BF) image (figure 2(*a*)) and the DF image (figure 2(*b*)) using the $\bar{1}10$ ferrite reflection show the ferrite precipitates with a specific orientation, the habit

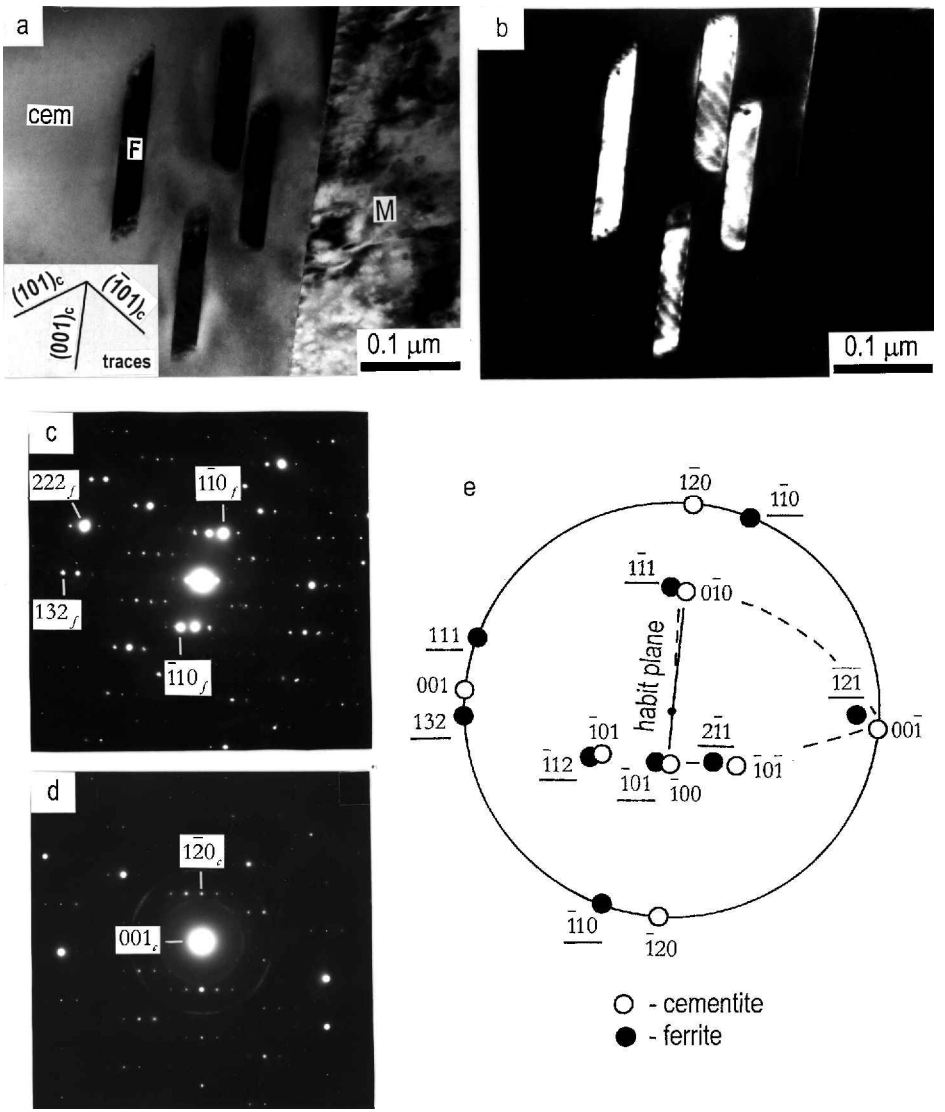

Figure 2. (*a*) BF image and (*b*) DF image using the $\bar{1}10_f$ reflection showing the ferrite precipitates within the cementite after heat treatment at 900°C for 100 s. (*c*), (*d*) SAD patterns taken from cementite regions with and without ferrite particles respectively. (*e*) Stereographic analysis. This is the Bagaryatsky orientation relationship when the ferrite habit plane is parallel to $(001)_c$.

planes being almost parallel to $(001)_c$ (within 3°). Figures 2(*c*) and (*d*) are the SAD patterns taken from cementite regions with and without ferrite precipitates. The stereographic analysis (figure 2(*e*)) of the SAD patterns shows that the orientation relationship between ferrite and cementite is close to that observed by Bagaryatsky (1950). The ferrite particles have a lath-like shape with the angle between the sides of about 56° as shown in figure 2(*a*). The sides are approximately parallel to $(121)_f // (001)_c$ and $(\bar{2}11)_f // (101)_c$ respectively.

Figure 3 is a series of transmission electron micrographs showing a ferrite lath formed in cementite. The incident beam direction is $[\bar{1}10]_f // [100]_c$. In the electron diffraction pattern in figure 3(*c*), the 001 reflection of cementite is on the line drawn

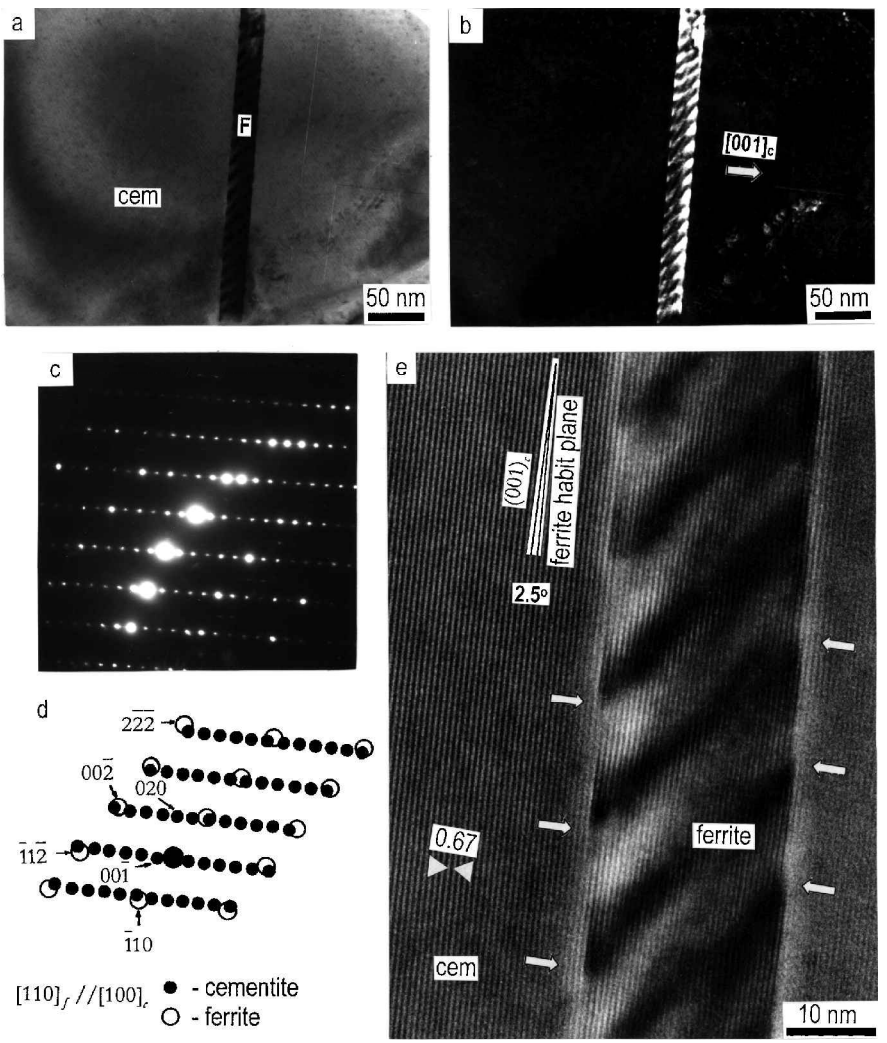

Figure 3. (*a*) BF image and (*b*) DF image using the $\bar{1}10$ reflection showing the ferrite precipitates within the cementite after heat treatment at 900°C for 100 s. (*c*) SAD pattern and (*d*) its schematic key diagram. (*e*) Cementite lattice image. This is the Bagaryatsky orientation relationship when the ferrite habit plane is parallel to $(001)_c$. The broad faces of the structural ledges are shown by white arrows.

through the centre and $1\bar{1}2$ reflection of ferrite; thus $(001)_c // (1\bar{1}2)_f$. The diffraction pattern and annotated diagram also show that $(010)_c // (\bar{1}11)_f$ and $[100]_c \approx // [110]_f$. Thus the ferrite relates to cementite by the Bagaryatsky orientation relationship. Figure 3(*e*) is a lattice image showing (001) cementite planes. The lattice fringes within the ferrite lath, which are parallel to the (001) cementite lattice image, may also arise from the cementite overlapping the ferrite. It can be seen that the ferrite habit plane deviates about 2.5° from $(001)_c // (\bar{1}12)_f$, which is the broad face on the habit plane. Figure 3(*e*) also shows that there are ledges on the ferrite–cementite interface aligning with regular spacing and height. The ledges are on both sides of the broad face of the ferrite lath and spaced such that the thickness of the ferrite lath is kept constant. The step height is equal to one unit lattice height of cementite in the [001] direction. The broad face of the ledges is of about 15 nm; thus these ledges are probably structural ledges (Hall *et al.* 1972) accommodating the deviation of the habit plane about 2.5° from the $(001)_c // (\bar{1}12)_f$ plane. Figures 3(*b*) and (*e*) also show the slanting fringe contrast arising between the structural ledges in the [110] direction of ferrite. This contrast appears to be the result of the strain fields between the structural ledges.

Figure 4 is the case of the Pitsch–Petch orientation relationship when the ferrite habit plane is precisely parallel to (001) cementite. In this figure, the ferrite–cementite interface is atomically flat. The ferrite and the cementite lattice images could not be resolved simultaneously in this figure but the variation in focus conditions revealed the $(\bar{1}10)_f$ lattice image of the region indicated by a circle in figure 4(*a*) as in the image inserted in figure 4(*d*) . This observation of a flat interface agrees well with the observation by Zhou and Shiflet (1991) of pearlite with the Pitsch–Petch orientation relationship. Figure 4(*d*) (inset) also shows that the ferrite–cementite interface at the tip of the lath is semicircular. This finding suggests that this is a projection of the growth direction of the ferrite lath that is normal to [001] cementite. Figure 5 shows the ferrite laths in the case of the Pitsch–Petch orientation relationship when ferrite habit planes are parallel to $(101)_c$.

Figure 6 shows a cementite particle that contains two sets of ferrite precipitates. Figures 6(*b*) and (*c*) are the SAD patterns taken from the ferrite precipitates labelled F_1 and F_2 respectively. The habit planes of the ferrite precipitates labelled F_2 were determined as $(101)_c$. The stereographic analysis in figure 6(*d*) shows that the orientation of these ferrite precipitates relative to cementite is close to the Bagaryatsky orientation relationship. It is interesting to note that Okamoto and Matsumoto (1975) reported the Isaichev (1947) orientation relationship in the case of the ferrite habit plane parallel to (101) cementite. The habit planes of the ferrite precipitates F_1 with respect to cementite are recognized as (001). The stereographic analysis reveals that this ferrite exhibits the Pitsch–Petch orientation relationship with cementite. It can also be seen that some of the ferrite laths remain in the martensite matrix after complete dissolution of the cementite (as shown by the arrow in the lower left corner of figure 6(*a*)).

Figure 7 shows the dislocation structure of ferrite that precipitated inside cementite after holding at 900°C for 100 s. The Bragg conditions $(\mathbf{g} = 110_f)$ are such that interface dislocations are well defined. The dislocation network is also observed at the left edge of the ferrite precipitate.

The present TEM investigation has shown that almost all cementite particles which remained after the fast and partial cementite dissolution controlled by carbon diffusion had nucleate ferrite laths within them. The density of ferrite precipitates

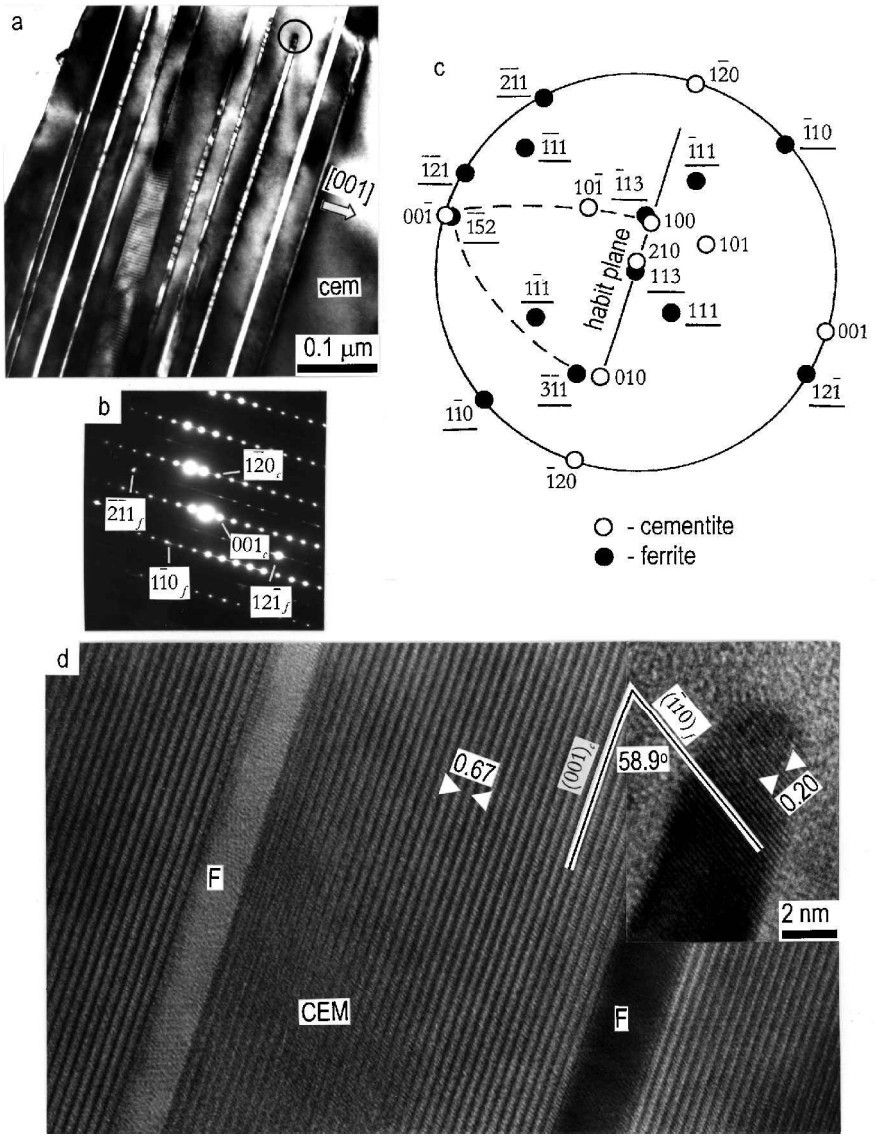

Figure 4. (*a*) BF image showing the ferrite precipitates with habit planes parallel to $(001)_c$ in the case of the Pitsch–Petch orientation relationship. (*b*) SAD pattern and (*c*) its stereographic analysis. (*d*) Cementite lattice image.

within cementite particles increases as the austenitizing temperature is raised (figure 8). All the particles observed were ferrite precipitates and no other phases were detected. Finally, it should be mentioned that ferrite precipitates were not observed within cementite particles after holding at 800° for periods from 100 to 10 000 s.

§4. Discussion

4.1. *Crystallography*

A second-phase precipitate formed within a matrix phase by an *in-situ* mechanism usually has a specific orientation relationship with respect to the matrix. It is well

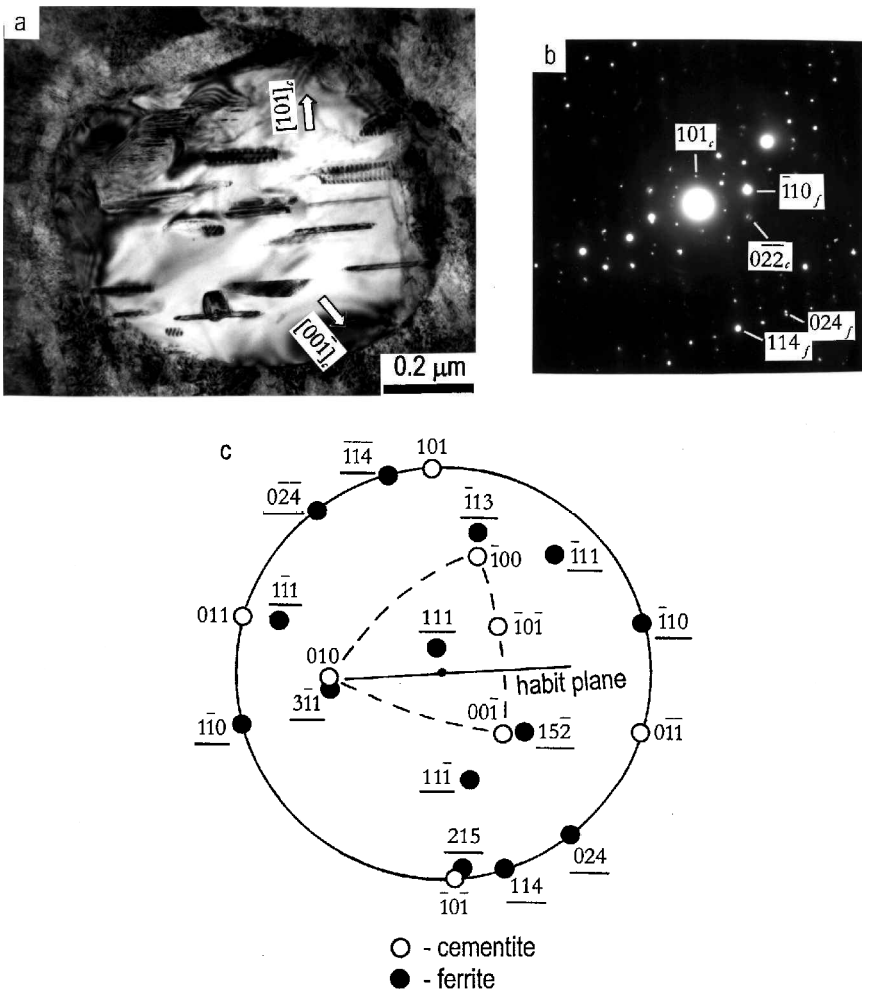

Figure 5. (*a*) BF micrograph showing the ferrite precipitates in the case of the Pitsch–Petch orientation relationship when ferrite habit planes observed are parallel to $(101)_c$. (*b*) SAD pattern and (*c*) its stereographic analysis.

known that there are three commonly reported orientation relationships between ferrite and cementite: the Pitsch (1962)–Petch (1953), the Bagaryatsky (1950) and the Isaichev (1947) relationships. The Pitsch–Petch and the Isaichev orientation relationships are frequently observed between ferrite and cementite in pearlite when both phases form from the parent austenite. It has often been reported that the Bagaryatsky orientation relationship exists between ferrite and cementite in ferrous pearlite (Whiting and Tsakiropoulos 1995a,b, Zhang and Kelly 1997b). The detailed examination of them, however, shows that the separation between the Bagaryatsky and the Isaichev orientation relationships is difficult to achieve in their patterns, that is, $[010]_\theta // \langle 111 \rangle_\alpha$ is rather far from the incident electron beam direction. Cementite precipitated from martensite during tempering reveals the Bagaryatsky orientation relationship with the matrix. In the present study both the Pitsch–Petch and the Bagaryatsky orientation relationships were found to exist between ferrite precipitates and cementite particles.

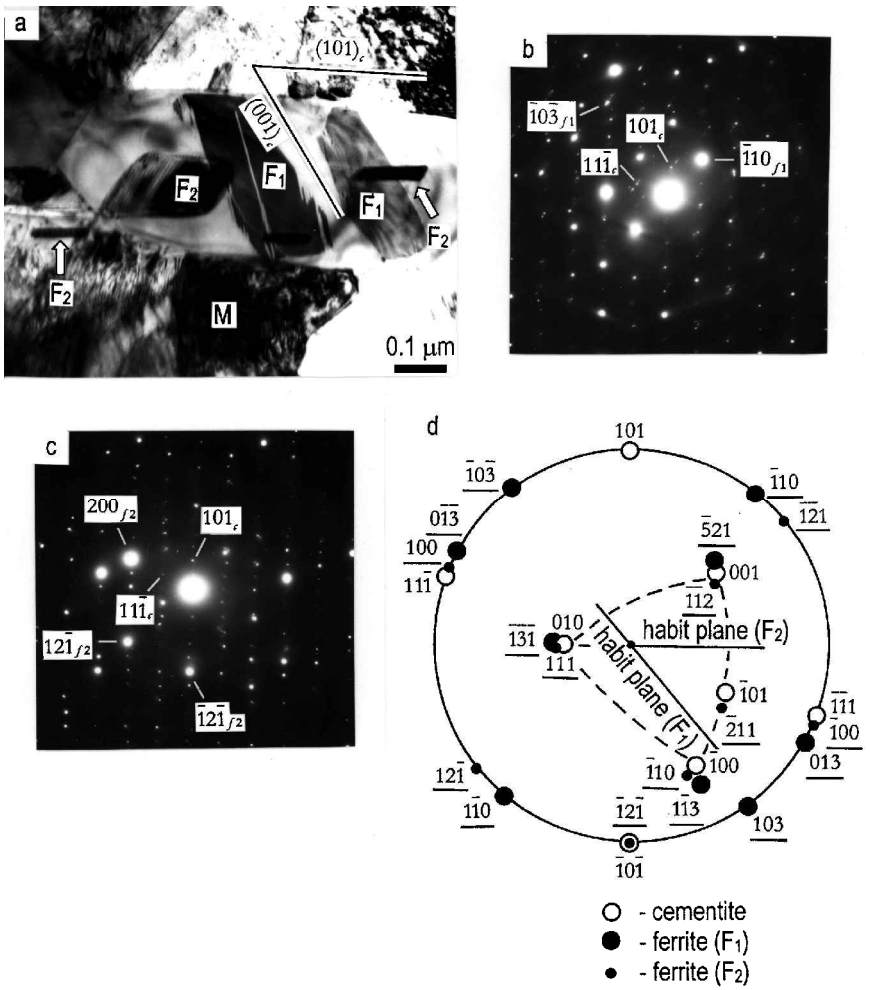

Figure 6. (*a*) BF micrograph showing the ferrite precipitates within cementite in the case of the Pitsch–Petch (laths labelled F_1) and the Bagaryatsky (F_2) orientation relationships. (*b*), (*c*) SAD patterns taken from ferrites F_1, and F_2 respectively. (*d*) Stereographic analysis.

The habit planes of the ferrite precipitates with respect to the cementite were established to be $(101)_c$ and $(001)_c$. The first finding agrees well with the results of Okamoto and Matsumoto (1975) whereas the second correlates with the results of Lyasotsky and Shtansky (1993). For each specific orientation relationship determined, both orientations of the habit planes were frequently observed. It is suggested that ferrite precipitates as a lath with the $(001)_c$ broad face and the $(101)_c$ side facet.

Figure 9 is a schematic diagram of the probable precipitation process of a ferrite lath within cementite. In the case of the Pitsch–Petch orientation relationship (figure 9(*a*)) the habit plane is assumed to be $(001)_c // (15\bar{2})_f$. The side facet of the ferrite lath is parallel to $(10\bar{1})_c // (21\bar{5})_f$. The angle between the $(00\bar{1})_c$ and $(101)_c$ planes of cementite is of 56.15° whereas that between the $(15\bar{2})_f$ and $(21\bar{5})_f$ planes is 55.48°. Thus the corresponding ferrite and cementite planes match with the accuracy of 0.33°. This suggests that the ferrite–cementite interface can be almost flat without any steps.

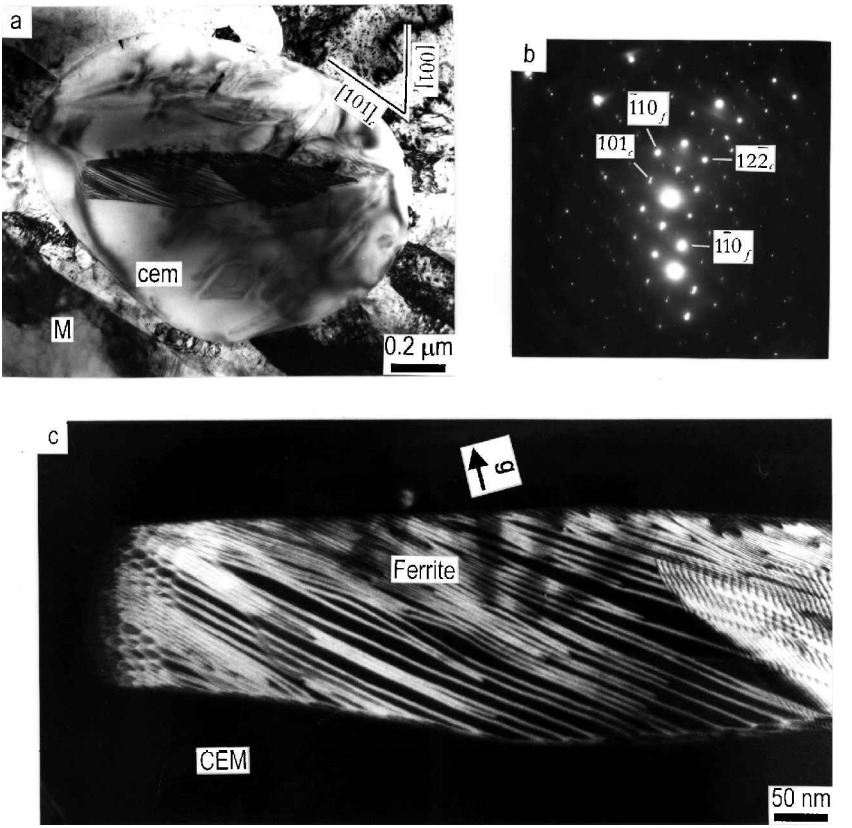

Figure 7. (*a*) BF image showing the dislocation structure of ferrite precipitated within cementite after heat treatment at 900°C for 100 s. (*b*) SAD diffraction pattern. Additional spots are due to the double diffraction. (*c*) DF image using $\mathbf{g} = 110_f$.

In the case of the Bagaryatsky orientation relationship (figure 9(*b*)) the habit plane is assumed to be $(001)_c // (\bar{1}12)_f$ and the side facet of the lath is parallel to $(101)_c // (\bar{1}21)_f$. In this case the angle between the $(\bar{1}12)_f$ and $(\bar{1}21)_f$ planes is 60° and it is suggested that the corresponding ferrite and cementite planes are not perfectly

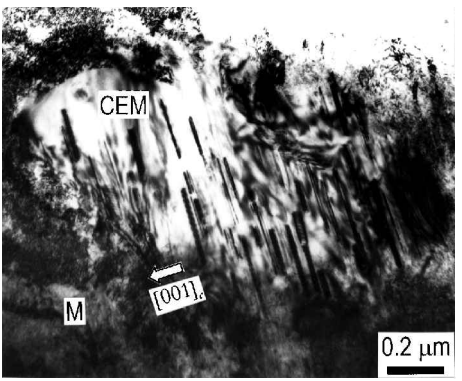

Figure 8. BF micrograph showing the ferrite precipitates after heat treatment at 950°C for 10 s.

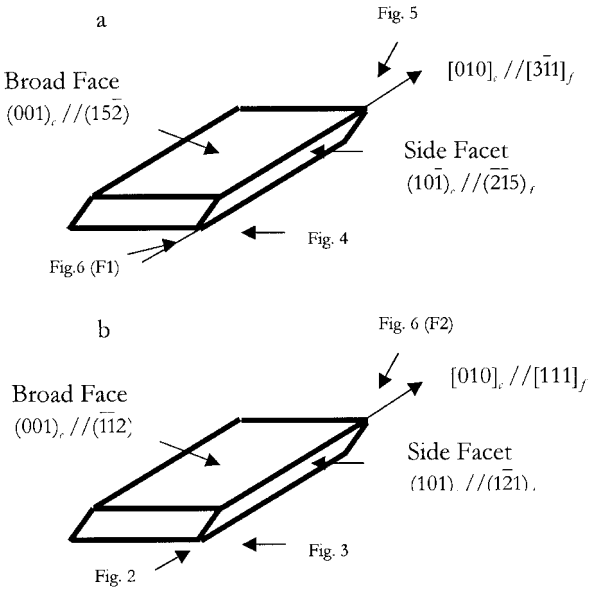

Figure 9. A schematic illustration of the morphology and the orientation of ferrite precipitates; (*a*) the Pitsch–Petch relationship; (*b*) the Bagaryatsky orientation relationship. The arrows also show the directions of the experimental observations.

matched. Thus structural ledges may exist at the ferrite–cementite interface to accommodate the misfit of the habit plane as shown in figure 10.

The possibility of austenite formation inside cementite with subsequent martensite transformation was proposed by Liu and Ågren (1991). It will be shown that the present results obtained exclude the possibility of austenite precipitation. Firstly, the formation of austenite within cementite seems to be questionable in comparison with that of ferrite simply in view of the lattice similarities between ferrite and cementite but not between austenite and cementite (Andrews 1963). Secondly, the martensitic formation of ferrite from austenite will destroy the shape of the austenite–cementite

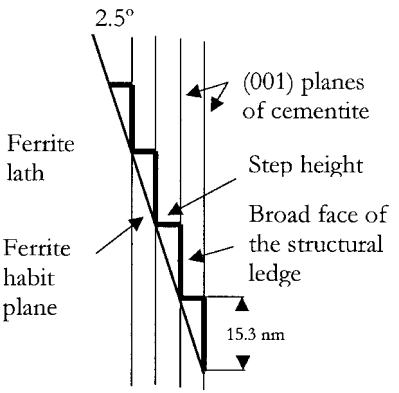

Figure 10. A schematic illustration of the structural ledges which accommodate the misfit of the ferrite habit plane of 2.5° from the atomistic habit plane $(112)_f // (001)_c$ in the case of the Bagaryatsky orientation relationship.

interface and it is thus difficult to see if the interface is smooth or facetted (Whiting and Tsakiropoulos 1995a,b, Zhou and Shiflet 1991, Hillert 1994). In the present study the structural ledges can be clearly seen by lattice image observation. Thirdly, it is only possible to observe the dislocation structure of ferrite presented in figure 7 if we assume that this ferrite has precipitated at a high temperature and has not undergone a $\gamma \rightarrow \alpha'$ transformation.

The orientation relationships determined between ferrite and cementite are the strongest evidence against the possibility of austenite precipitation within cementite particles. Only one orientation relationship between cementite and austenite has frequently been reported in the literature (Pitsch 1962):

$$(100)_c // (5\bar{5}4)_\gamma, (010)_c // (110)_\gamma, (001)_c // (\bar{2}25)_\gamma,$$

although a new orientation relationship has recently been reported by Zhou and Shiflet (1992):

$$(100)_c // (23\bar{1})_\gamma, (010)_c // (013)_\gamma, (001)_c // (5\bar{3}1)_\gamma.$$

If the cementite was related to austenite by the Pitsch (1962) relationship, then subsequent transformation of austenite to martensite (assuming the Kurdjumov–Sachs relationship) would yield a relationship several degrees away from the Bagaryatsky relationship. The new relationship reported by Zhou and Shiflet (1992) would yield neither of the observed ferrite–cementite relationships on transformation of austenite to martensite. Thus, neither the Bagaryatsky nor the Pitsch–Petch relationships is consistent with the precipitation of austenite followed by a martensitic reaction.

4.2. *Mechanism of ferrite precipitation*

From the results obtained, it is evident that the nature of ferrite precipitates in the present study is somewhat different from that in the experiments of Okamoto and Matsumoto (1975). The temperatures at which the number of particles in the eutectic cementite became a maximum in their experiments were 400–500°C and higher temperatures suppressed the precipitation reaction.

According to Ågren and Vassilev (1984) the dissolution of cementite in chromium-alloyed steels can be divided into three stages: the rate of the first stage is controlled by carbon diffusion in austenite, the second stage by chromium diffusion in carbides and the third stage by chromium diffusion in austenite. As was pointed out by Omsen and Liljestrand (1972), any experimental evidence for the second stage is difficult to find. This classification of the process will be basis for the discussion of the precipitation of ferrite within cementite. The following discussion will be based on the thermodynamic equilibrium calculations that have been performed with the software and database THERMOCALC (Hillert 1981).

Figures 11 (*a*) and (*b*) show the calculated isothermal section of the Fe–Cr–C phase diagram at 900°C, representing the metastable $\alpha + \gamma +$ cem three-phase equilibrium with respect to different types of horizontal axis, (*a*) carbon content and (*b*) carbon activity. No other phases have been observed in the present study and thus they have been omitted. The dotted curves show calculated metastable extension of the $\alpha +$ cementite two-phase equilibrium. The slanting broken line starting from the open star defines the initial equilibrium after tempering at 735°C for 240 h.

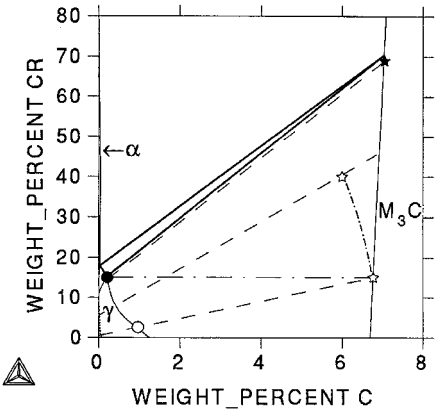

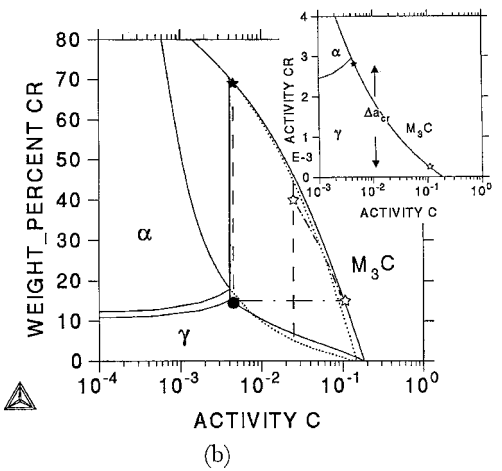

Figure 11. Calculated isothermal section of the Fe–Cr–C phase diagram at 900°C representing the metastable $\alpha + \gamma + M_3C$ three-phase equilibrium: (*a*) weight percentage of carbon and (*b*) carbon activity as the horizontal axis; (' ' '), calculated metastable extension of $\alpha + M_3C$ two-phase equilibrium; (- - - -), the tie-lines of the $\alpha + M_3C$ and $\gamma + M_3C$ equilibria; (—' —), defines the composition of austenite if it inherited the chromium content of the cementite. The composition of alloy is shown by open circle. All the other lines and symbols are explained in §4.2.

During the first stage the $\alpha \rightarrow \gamma$ transformation is completed and the cementite particles dissolve partially within the austenite matrix. Carbon atoms diffuse into the austenite matrix very rapidly in comparison with chromium atoms and the austenite in the vicinity of the partially dissolved cementite particle will inherit the chromium content from the carbide (as shown by the horizontal dash-dotted line in figures 11(*a*) and (*b*)). When the first stage is completed, the activity of carbon becomes uniform within the material and the following reaction is controlled by chromium diffusion. According to the assumption local equilibrium at the interface, the operative tie-line of the reaction at the γ–cementite interface is thus given by the slanting broken line joining the full circle and full star. Thus the concentration spike at the γ–cementite interface must be assumed to exist in order to fulfill the condition of local equilibrium. Such a compositional spike is frequently reported in the literature when

the dissolution of alloy carbides in austenite is treated mathematically (Liu *et al.* 1991, Shtansky and Inden 1997). Direct experimental evidence of chromium enrichment in the outer layer of dissolving cementite in Fe–Cr–C alloys was obtained by Liu and Ågren (1991) using energy-dispersive spectroscopy techniques.

In the centre of the cementite particle and in the surrounding austenite matrix far away from the carbide, the chromium content does not change. In principle, the chromium atoms can diffuse both towards the centre of the cementite and away from the γ–cementite interface into the austenite matrix. Figure 11(*b*) shows the chromium activity difference between the γ–cementite interface and the bulk cementite. This chromium activity difference acts as a strong driving force for the diffusion of chromium atoms from the γ-cementite interface towards the centre of the cementite particle. It seems reasonable that the composition of cementite is stoichiometric with respect to carbon and that iron atoms can be replaced by chromium atoms to produce $(Fe, Cr)_3C$. If the diffusion of chromium occurs within cementite, the excess of metal atoms will result in the precipitation of ferrite. In such a situation, cementite can be considered as a supersaturated solid solution with respect to metal atoms.

The formation of ferrite also requires carbon diffusion from the ferrite–cementite interface since the carbon content of ferrite is considerably lower than that of cementite. The chromium content in ferrite precipitates is unknown. However, the diagram in figure 11(*b*) shows that any chromium content in ferrite higher than in cementite (the corresponding operative tie-line located on the left of the γ-cementite tie-line joining the points (●) and (★)) gives the opposite direction for chromium and carbon diffusion within cementite. Thus the corresponding tie-line has to be located on the right. This agrees well with the average chromium content in the precipitated plates reported by Liu and Ågren (1991). The composition of cementite that receives chromium from the γ-cementite interface will change along the curved dash-dotted line, shown schematically in figure 11. This cementite becomes non-stoichiometric with respect to carbon and thus can decompose with the formation of stoichiometric cementite and ferrite as shown by slanting broken line in figure 11(*a*). It is suggested that, despite the fact that the cementite's composition lies in the γ + cementite phase field, the metastable ferrite nucleates in favour of austenite. Such kinetic barriers to precipitation of equilibrium phases are well known (for example Hillert (1975)).

§ 5. Conclusions

The mechanism and the crystallography of the ferrite laths precipitated from the cementite were studied in an Fe–2.6 wt% Cr–0.96 wt% C alloy at different austenitizing temperatures 800–950°C. The following results were obtained.

(1) Ferrite precipitates relate to cementite either by the Pitsch–Petch or by the Bagaryatsky orientation relationship.
(2) Ferrite particles precipitate as laths elongated in the [010] direction of cementite.
(3) In the case of the Pitsch–Petch orientation relationship, the habit plane of a ferrite lath is parallel to $(\bar{1}\bar{5}2)_f // (001)_c$. The side facet of the lath is close to $(\bar{2}\bar{1}5)_f // (10\bar{1})_c$ and the ferrite growth direction is close to $[\bar{3}11]_f // [010]_c$.
(4) In the case of the Bagaryatsky orientation relationship, the habit plane of a ferrite lath deviates several degrees from the $(\bar{1}\bar{1}2)_f // (001)_c$. The side facet of the lath is close to $(\bar{1}2\bar{1})_f // (10\bar{1})_c$ and the ferrite growth direction is close to $[\bar{1}\bar{1}1]_f // [010]_c$.

(5) In the case of the Bagaryatsky orientation relationship, structural ledges form on the {112} broad face of the ferrite lath to preserve the lath habit plane.
(6) The mechanism of the observed reaction can be qualitatively understood by assuming the local equilibrium at the γ–cementite and α–cementite interfaces. This approach predicts a strong diffusion of chromium atoms from the γ-cementite interface towards the centre of the cementite, resulting in the precipitation of excess metal atoms within cementite.
(7) The growth of ferrite precipitates is controlled by chromium diffusion in cementite.

Acknowledgements

D. S. acknowledges the support of the Japan Society for the Promotion of Science during this work. This research was supported by the Grant-in-Aid of The Ministry of Education, Science, Culture and Sports. Thanks are also due to Sumitomo Metal Industries for supplying the materials used in the present study.

References

Ågren, J., and Vassilev, G., 1984, *Mater. Sci. Engng.,* **64**, 95.
Andrews, K. W., 1963, *Acta metall.,* **11**, 939.
Bagaryatsky, Y. A., 1950, *Dokl. Akad. Nauk. SSSR,* **73**, 1161.
Hall, M. G., Aaronson, H. I., and Kinsman, K. R., 1972, *Surf. Sci.*, **31**, 257.
Hillert, M., 1975, *Lectures on the Theory of Phase Transformation,* edited by H. I. Aaronson (Warrendale, Pennsylvania: Metallurgical Society of AIME), p. 1; 1981, *Proceedings of the International Conference on Solid–Solid Phase Transformations*, Carnegie Mellon University (Metallurgical Society of AIME), p. 789; 1994, *Scripta metall.,* **31**, 1173.
Hillert, M., and Uhrenius, B., 1972, *Scand. J. Metall.,* **1**, 223.
Inoue, A., and Matsumoto, T., 1980, *Metall. Trans.* A, **11**, 739.
Isaichev, I. V., 1947, *Zh. Tekh. Fiz.,* **17**, 835.
Kurdjumov, G. V., and Sachs, G., 1930, *Z. Phys.,* **64**, 325.
Liu, Z.-K., and Ågren, J., 1991, *Metall Trans.* A, **22**, 1753.
Liu, Z.-K., Höglund, L., Jönsson, B., and Ågren, J., 1991, *Metall. Trans.* A, **22**, 1745.
Lyasotsky, I. V., and Shtansky, D. V., 1993, *Phys. Metals Metallogr.* (USSR), **75**, 1, 53, 77.
Okamoto, T., and Matsumoto, H., 1975, *Metal Sci.,* **9**, 8.
Omsén, A., and Liljestrand, L.-G., 1972, *Scand. J. Metall.,* **1**, 241.
Petch, N. J., 1953, *Acta crystallogr.,* **6**, 96.
Pitsch, W., 1962, *Acta metall.,* **10**, 897.
Shtansky, D. V., and Inden, G., 1997, *Acta mater.,* **45**, 7, 2879.
Whiting, M. J., and Tsakiropoulos, P., 1995a; *Scripta metall. mater.,* **32**, 1965; 1995b, *Mater. Sci. Technol.,* **11**, 717.
Zhang, M.-X., and Kelly, P. M., 1997, *Scripta mater.,* **37**, 2009.
Zhou, D. S., and Shiflet, G. J., 1991, *Metall. Trans.* A, **22**, 1349; 1992, *Scripta metall.,* **27**, 1215.